Rotor Dynamics of Polygonal Mirror Scanner Motor Supported by Air Bearings in Digital Electrophotography

Hiroyuki Kawamoto

Foundation Research Laboratory, Corporate Research Laboratories, Fuji Xerox Co., Ltd., 430 Sakai, Nakai-machi, Ashigarakami-gun, Kanagawa 259-01, Japan

A mathematical analysis has been performed on rotor dynamics of a high-speed polygonal mirror scanner motor in digital electrophotography. The rotor is assumed rigid and vertically supported by air bearings with an effective length that is not negligible compared to the rotor length. The model is a four-degree-of-freedom system that includes the gyroscopic effect and nonorthogonal force of the air bearing. The model also includes the effects of longitudinal bearing length and radially unstable magnetic stiffness of a driving motor and/or a magnetic bearing. A simulation program was coded to calculate complex eigenvalues, static and dynamic stability, critical speeds, unbalance responses, and external excitation responses. The results indicated that although the effects of bearing length and magnetic unstable stiffness were ignored in the past, these simplifications result in substantial error for the evaluation of rotor dynamics. The model is utilized to realize high-performance scanner motors.

Journal of Imaging Science and Technology 41: 565–569 (1997)

Introduction

A polygonal mirror scanner motor is used in the exposure subsystem of digital xerography to scan a laser beam and to write latent images on the photoreceptor.[1] The rotation of the mirror must have (1) stable, constant velocity and low vibration to realize high image quality, (2) high-speed rotation for high print speed and high-resolution machines, (3) long life, (4) small heat loss, and (5) low acoustic noise. Instead of conventional ball bearings, self-acting herringbone-grooved air bearings are used to meet these requirements,[2] in particular for high-speed machines. The self-acting grooved air bearing was developed to suppress the instability of non-grooved bearings and is being utilized not only for laser scanner motors but also for videotape recorders. Its fundamental statics and dynamics were originally investigated by Vohr and Chow[3] based on a smoothed overall pressure distribution model in the 1960s, and then many numerical methods were proposed for the practical design of the bearing as reviewed by Castelli and Pirvics.[4] Nevertheless, we can utilize charts calculated by Hamrock and Fleming[5] to design the optimal bearing for maximum radial load capacity without numerical calculations.

Three major differences exist between ball and air bearings with respect to rotor dynamics. The first is that the reaction force induced by an air film of the air bearing is not orthogonal, i.e., displacement direction of a shaft does not coincide with the force direction of the bearing. It is well known that this induces dynamic instability called "half-frequency whirl" and extensive theoretical and experimental work has been done to realize highly stable bearing rotor systems.[6–8] The second difference is that the stiffness of the gas bearing is not induced without rotation and is small in the low-speed region. Because magnetic negative stiffness is induced by the motor and a passive thrust magnetic bearing[9,10] even at zero speed, total stiffness of the rotor system is negative and the rotor is statically unstable in the very low-speed region. This induces dry contact between the rotor and shaft at speeds lower than the threshold, and the lifetime of the bearing is reduced by the frequent start–stop operation. The third difference is that the effective axial length of the air bearing is not negligibly short compared to the rotor length. Figure 1 shows a typical scanner motor supported by gas journal bearings. The total length of the two bearings is almost 80% of the rotor length. Although extensive work has been done to simulate rotor dynamics supported by journal bearings, the status ignored the length of the air bearing.[11–14] The conventional assumption is that the concentrated reaction force is applied at the center of the journal bearing. This simplification results in substantial error in some cases for the evaluation of rotor dynamics.

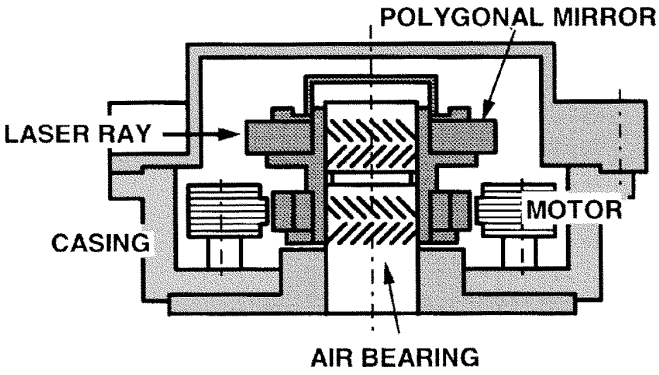

Figure 1. Configuration of a polygonal mirror scanner motor supported by air bearings.

Original manuscript received February 19, 1997

A modified mathematical model is presented in this report to realize a sophisticated design on the rotor dynamics of the scanner motor supported by air bearings. The model is a four-degree-of-freedom system that includes not only the gyroscopic effect and non-orthogonal force of the air bearing but also the effects of longitudinal bearing length and radially unstable magnetic stiffness of the driving motor and/or magnetic bearing. A simulation program was coded to calculate complex eigenvalues, static and dynamic stability, critical speeds, unbalance responses, and external excitation responses. It was indicated how bearing length and magnetic unstable stiffness, which have been ignored in the past, influence rotor dynamics and stability. The model is utilized to realize high-performance scanner motors.

Vibration Model

The following simplifications were made to derive a simple but realistic linear vibration equation:

(1) The rotor, mass m, the polar moment of inertia I_p, and the lateral moment of inertia I_d, is rigid and axisymmetric, but a small static unbalance ε and dynamic unbalance τ exist in the rotor.
(2) Because the rotor is vertically supported, bearing forces are assumed isotropic.
(3) The effect of gravity is neglected.
(4) Two kinds of bearings are defined: one is concentrated, such as the ball bearing with force acting on a concentrated position of the rotor, and the other is distributed bearing with substantial length compared with the rotor, such as the air bearing and the electrical motor. The bearing force in the distributed bearing is assumed to be uniformly distributed in the axial direction.
(5) The displacement and the gradient of the rotor are small to satisfy the linearity. The bearing force is also assumed to be linear with respect to the displacement and the gradient of the rotor.
(6) A casing on a coordinate o-x,y,z is excited and moves in the lateral direction (X_0, Y_0) and leans (Θ_x, Θ_y) from a stationary coordinate 0-XYZ.
(7) The rotational speed ω is constant.

The system configuration is shown in Fig. 2. Because the rotor is assumed rigid, the system has four degrees of freedom $(x, y, \theta_x, \theta_y)$.

Vibration Equation

A fundamental vibration equation corresponding to the model is[10]

$$\mathbf{M}\ddot{\mathbf{X}} + (\mathbf{C} + \omega\mathbf{L})\dot{\mathbf{X}} + \mathbf{K}\mathbf{X} = \mathbf{F}, \tag{1}$$

where

$$\mathbf{X} = (\underline{r}, \underline{\theta})^T = (x + iy, \theta_x + i\theta_y)^T \quad \left(i = \sqrt{-1}\right), \tag{2}$$

$$\mathbf{M} = \begin{pmatrix} m & 0 \\ 0 & I_d \end{pmatrix}, \tag{3}$$

$$\mathbf{L} = \begin{pmatrix} 0 & 0 \\ 0 & -iI_p \end{pmatrix}, \tag{4}$$

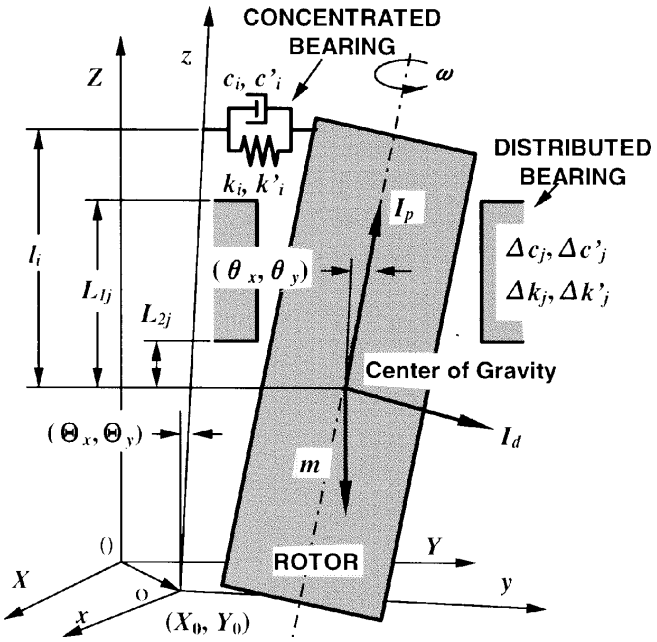

Figure 2. Vibration model.

$$\mathbf{C} = \begin{pmatrix} C - iC' & C_{r\theta} - iC'_{r\theta} \\ \text{Sym.} & C_\theta - iC'_\theta \end{pmatrix}, \tag{5}$$

$$\mathbf{K} = \begin{pmatrix} K - iK' & K_{r\theta} - iK'_{r\theta} \\ \text{Sym.} & K_\theta - iK'_\theta \end{pmatrix}. \tag{6}$$

Here, **M** is a mass-inertia matrix, **C** is a damping matrix, **L** is a gyroscopic matrix, **K** is a stiffness matrix, **X** is a displacement-gradient vector, $\dot{x} \equiv dx/dt$, $\ddot{x} \equiv d^2x/dt^2$, and t is time. The superscript T indicates a transposed vector and the underline means complex. An external force vector **F** consists of the unbalance force and the casing excitation force.

$$\begin{aligned} \mathbf{F} = &\left(\varepsilon m\omega^2 e^{i\omega t}, \tau(I_d - I_p)\omega^2 e^{i(\omega t+\alpha)}\right)^T - \\ &- \mathbf{M}\ddot{\mathbf{X}}_0 - \omega\mathbf{L}\dot{\mathbf{X}}_0, \mathbf{X}_0 = (X_0 + iY_0, \Theta_x + i\Theta_y)^T, \end{aligned} \tag{7}$$

where α is an angle between the static and dynamic unbalance positions. Because the damping and the stiffness of the distributed bearing are derived by the equation,

$$\begin{aligned} c_q, k_q = &\frac{\partial}{\partial q}\left[\frac{1}{2}\Delta c, k\int_{L_2}^{L_1}\left\{(x + \theta_x z)^2 + (y + \theta_y z)^2\right\}dz\right] \\ &\left(q = \dot{x}, \dot{y}, \dot{\theta}_x, \dot{\theta}_y \text{ for } c,\ q = x, y, \theta_x, \theta_y, \text{ for } k,\right), \end{aligned} \tag{8}$$

elements in the damping and stiffness matrices are expressed as follows:

$$C = \sum_{i=1}^{n} c_i + \sum_{j=1}^{m} \Delta c_j \left|L_{1j} - L_{2j}\right|, \quad K = \sum_{i=1}^{n} k_i + \sum_{j=1}^{m} \Delta k_j \left|L_{1j} - L_{2j}\right|, \tag{9}$$

$$C' = \sum_{i=1}^{n} c_i' + \sum_{j=1}^{m} \Delta c_j' \left| L_{1j} - L_{2j} \right|, \quad K' = \sum_{i=1}^{n} k_i' + \sum_{j=1}^{m} \Delta k_j' \left| L_{1j} - L_{2j} \right|, \tag{10}$$

$$C_\theta = \sum_{i=1}^{n} c_i \ell_i^2 + \frac{1}{3} \sum_{j=1}^{m} \Delta c_j \left| L_{1j}^3 - L_{2j}^3 \right|,$$
$$K_\theta = \sum_{i=1}^{n} k_i \ell_i^2 + \frac{1}{3} \sum_{j=1}^{m} \Delta k_j \left| L_{1j}^3 - L_{2j}^3 \right|, \tag{11}$$

$$C_\theta' = \sum_{i=1}^{n} c_i' \ell_i^2 + \frac{1}{3} \sum_{j=1}^{m} \Delta c_j' \left| L_{1j}^3 - L_{2j}^3 \right|,$$
$$K_\theta' = \sum_{i=1}^{n} k_i' \ell_i^2 + \frac{1}{3} \sum_{j=1}^{m} \Delta k_j' \left| L_{1j}^3 - L_{2j}^3 \right|, \tag{12}$$

$$C_{r\theta} = \sum_{i=1}^{n} c_i \ell_i + \frac{1}{2} \sum_{j=1}^{m} \Delta c_j \left| L_{1j}^2 - L_{2j}^2 \right|,$$
$$K_{r\theta} = \sum_{i=1}^{n} k_i \ell_i + \frac{1}{2} \sum_{j=1}^{m} \Delta k_j \left| L_{1j}^2 - L_{2j}^2 \right|, \tag{13}$$

$$C_{r\theta}' = \sum_{i=1}^{n} c_i' \ell_i + \frac{1}{2} \sum_{j=1}^{m} \Delta c_j' \left| L_{1j}^2 - L_{2j}^2 \right|,$$
$$K_{r\theta}' = \sum_{i=1}^{n} k_i' \ell_i + \frac{1}{2} \sum_{j=1}^{m} \Delta k_j' \left| L_{1j}^2 - L_{2j}^2 \right|, \tag{14}$$

where c and k are the damping and stiffness of the concentrated bearings; Δc and Δk are the damping and stiffness per unit length of the distributed bearings; L_1 and L_2 are the distances from the gravitational center of the rotor to the upper and lower end of the distributed bearings; l is the distance from the gravitational center of the rotor to the concentrated bearings; n and m are the numbers of concentrated and distributed bearings, respectively; and the superscript " ′ " means nonorthogonal.

Effect of Bearing Length

Because $\Delta c \left| L_1 - L_2 \right| = c$ and $\Delta k \left| L_1 - L_2 \right| = k$, the second terms on the right sides of Eqs. 9, 10, 13, and 14 are equal to the constants when the bearing force is applied to the center of the bearing. This means that bearing length does not affect the dynamics related to the cylindrical mode, even if the force is assumed to be applied to the center of the bearing. But because the ratio of the second terms on the right sides of Eqs. 11 and 12 to that with the concentrated bearing assumption is

$$R \equiv \frac{\frac{1}{3} \Delta k \left| L_1^3 - L_2^3 \right|}{k \left\{ \frac{(L_1 + L_2)}{2} \right\}^2} = \frac{4}{3} \left[1 - \frac{\frac{L_2}{L_1}}{\left(1 + \frac{L_2}{L_1} \right)^2} \right], \tag{15}$$

the bearing length affects the dynamics of the conical mode. Figure 3 shows how L_2/L_1 affects $R^{1/2}$, which is proportional to the damping ratio, natural frequency, and critical speed of the conical mode. Clearly, these parameters are underestimated for the concentrated assumption of the gas bearing.

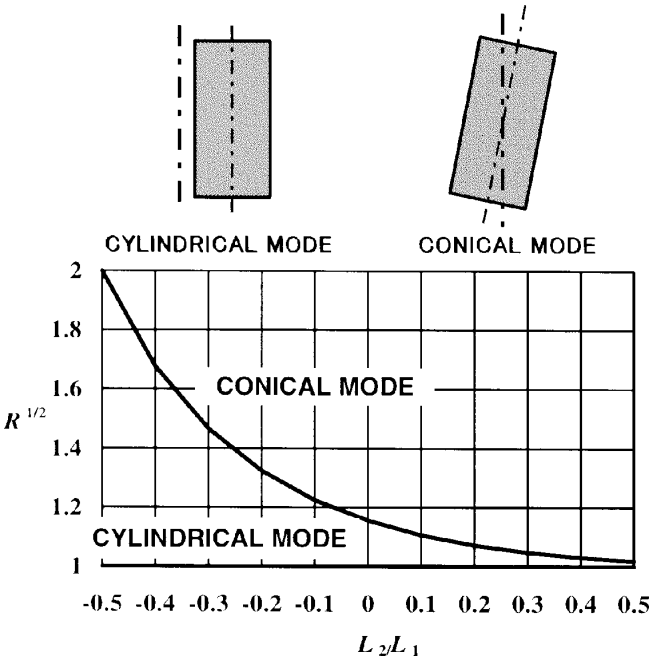

Figure 3. Mode shapes and effect of bearing length.

Complex Eigenvalues and Stability

Substitution of the free vibration solution $r = r_0 \exp(\lambda t)$, $\theta = \theta_0 \exp(\lambda t)$ into Eq. 1 gives the following characteristic equation:

$$(a_4 + ib_4)\lambda^4 + (a_3 + ib_3)\lambda^3 + (a_2 + ib_2)\lambda^2 + (a_1 + ib_1)\lambda + a_0 + ib_0 = 0, \tag{16}$$

where

$$a_4 = mI_d,$$
$$b_4 = 0,$$
$$a_3 = mC_\theta + I_d C,$$
$$b_3 = -mC_\theta' - \omega m I_p - I_d C',$$
$$a_2 = mK_\theta + CC_\theta - C'(C_\theta' + \omega I_p) + I_d K - C_{r\theta}^2 + C_{r\theta}'^2,$$
$$b_2 = -K_\theta' + C'C_\theta - C(C_\theta' + \omega I_p) - I_d K' + 2C_{r\theta}C_{r\theta}',$$
$$a_1 = KC_\theta - K'(C_\theta' + \omega I_p) + K_\theta C - K_\theta' C' - 2K_{r\theta}C_{r\theta} + 2K_{r\theta}'C_{r\theta}',$$
$$b_1 = -K'C_\theta - K(C_\theta' + \omega I_p) - K_\theta' C - K_\theta C' + 2K_{r\theta}C_{r\theta}' + 2K_{r\theta}'C_{r\theta},$$
$$a_0 = KK_\theta - K'K_\theta' - K_{r\theta}^2 + K_{r\theta}'^2,$$
$$b_0 = -KK_\theta' - K'K_\theta + 2K_{r\theta}K_{r\theta}'.$$

The Newton-Raphson method was used to solve Eq. 16. Four sets of the natural frequency ω_0 and modal damping ζ_0 are calculated from the four complex eigenvalues $\lambda = \lambda_r + i\lambda_i$.

$$\omega_0 = \lambda_i, \quad \zeta_0 = \frac{-\lambda_r}{\sqrt{\lambda_r^2 + \lambda_i^2}}. \tag{17}$$

A pair of complex eigenvalues corresponds to the cylindrical mode and the other pair corresponds to the conical mode. The mode shapes are shown in Fig. 3. One of each mode is forward, if its natural frequency is positive, and backward in the case of negative frequency. Here,

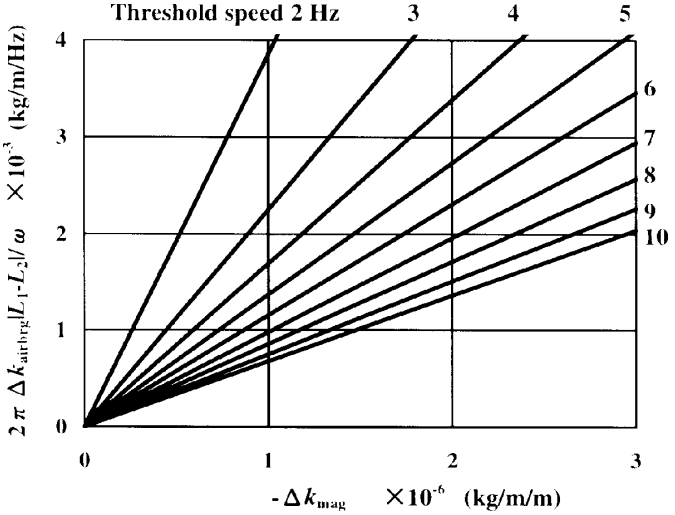

Figure 4. Statically unstable threshold speed caused by magnetic negative stiffness of the electrical motor. The rotor is supported by two air bearings, airbrg1 and airbrg2, and the stiffness of the air bearing is assumed proportional to the speed.

forward means that the direction of the whirling vibration is the same as the rotational direction and backward means that the rotor whirls in opposite direction to the rotational direction. Due to the gyroscopic effect, the forward whirling frequency increases and the backward decreases in accordance with the increase of rotation speed. If the modal damping is negative, the corresponding mode is dynamically unstable. It is well known that nonorthogonal stiffness k' and $\Delta k'$ reduces the forward whirling stability.[11–13] However, the results of numerical calculations confirm that damping of the gas bearing is usually large enough to compensate for the dynamic instability due to nonorthogonal stiffness and the rotor is sufficiently stable. This coincides with the experimental result that no self-excited vibration occurred in the actual rotor.

But, negative stiffness of the radial-stable-type passive magnetic bearing and/or the cylindrical motor makes the rotor supported by the air bearings statically unstable at very low speeds, because stiffness of air bearings is not induced without rotation, which is small in the low speed region, whereas magnetic negative stiffness exists even at zero speed. Dry contact between the rotor and shaft is induced at speeds lower than the threshold. Figure 4 shows an example of the calculated relationship among the threshold frequency, the negative stiffness of the motor, and the stiffness of the air bearing. Parameters used for the calculation were; mg = 0.16 kg, $I_d g$ = 3.64×10^{-6} kgm^2, $I_p g$ = 2.62×10^{-6} kgm^2, $L_{1\text{mag}} = -10.55 \times 10^{-3}$ m, $L_{2\text{mag}} = 16.15 \times 10^{-3}$ m, $L_{1\text{airbrg1}} = 3 \times 10^{-3}$ m, $L_{2\text{airbrg1}} = 23 \times 10^{-3}$ m, $L_{1\text{airbrg2}} = -1 \times 10^{-3}$ m, and $L_{2\text{airbrg2}} = -21 \times 10^{-3}$ m. These values correspond to the actual motor shown in Fig. 1. Because dry contact reduces the lifetime of the air bearing, it is preferable to avoid frequent start–stop operation and to keep the rotor speed higher than the threshold.

Critical Speed

Critical speed is when the forward whirling frequency coincides with the rotation frequency. Two critical speeds exist: the lower corresponds to the cylindrical mode and the higher corresponds to the conical mode. The rotor is usually operated under the first critical speed, i.e., the system is designed to be sub-critical. This also coincides with the experimental observation that no resonance peak of the vibration, which synchronized with the rotational frequency, was observed below the operation frequency 600 Hz.

Unbalance Response

Unbalance response is calculated by the following equations:

$$\underline{r} = \underline{r}_0 \exp(i\omega t),\ \ \underline{\theta} = \underline{\theta}_0 \exp(i\omega t), \tag{18}$$

where

$$\underline{r}_0 = \frac{1}{\underline{D}}\begin{vmatrix} \varepsilon m\omega^2 & (C_{r\theta} - iC'_{r\theta})i\omega + K_{r\theta} - iK'_{r\theta} \\ \tau(I_d - I_p)\omega^2 e^{i\alpha} & -(I_d - I_p)\omega^2 + (C_\theta - iC'_\theta)i\omega + K_\theta - iK'_\theta \end{vmatrix},$$

$$\underline{\theta}_0 = \frac{1}{\underline{D}}\begin{vmatrix} -m\omega^2 + (C - iC')i\omega + K - iK' & \varepsilon m\omega^2 \\ (C_{r\theta} - iC'_{r\theta})i\omega + K_{r\theta} - iK'_{r\theta} & \tau(I_d - I_p)\omega^2 e^{i\alpha} \end{vmatrix},$$

$$\underline{D} = \begin{vmatrix} -m\omega^2 + (C - iC')i\omega + K - iK' & (C_{r\theta} - C'_{r\theta})i\omega + K_{r\theta} - iK'_{r\theta} \\ \text{Sym.} & -(I_d - I_p)\omega^2 + (C_\theta - iC'_\theta)i\omega + K_\theta - iK'_\theta \end{vmatrix}.$$

The reaction force per unit length of the bearing $\underline{f}_{brj}$ at j is

$$\underline{f}_{brj} = -\left\{\Delta k_j + \omega\Delta c'_j - i\left(\Delta k'_j - \omega\Delta c_j\right)\right\}\underline{r}_{0j} \exp(i\omega t). \tag{19}$$

Integration of Eq. 19 gives total reaction force $\underline{F}_{brj}$ of the gas gearing.

$$\begin{aligned} \underline{F}_{brj} &= \int_{L_{2j}}^{L_{1j}} \underline{f}_{brj}\, dz \\ &= -\left\{\Delta k_j + \omega\Delta c'_j - i\left(\Delta k'_j - \omega\Delta c_j\right)\right\} \\ &\quad \left\{\left(L_{1j} - L_{2j}\right)\underline{r}_0 + \frac{1}{2}\left(L_{1j}^2 - L_{2j}^2\right)\underline{\theta}_0\right\} \exp(i\omega t). \end{aligned} \tag{20}$$

Characteristics of the unbalance response have been reported elsewhere.[14,15]

External Excitation Response

The general external excitation response is numerically calculated as an initial value problem using the Runge-Kutta method. Because the external excitation force usually contains not only forward but also backward components and its frequency is not the same as the rotation frequency, the response also contains backward and forward whirling not synchronized with the rotational frequency.[10,15] These characteristics are largely different from those of the unbalance response. These issues will be reported in a separate study.

Conclusion

Rotor dynamics of the polygonal mirror scanner motor supported by air bearings have been mathematically

investigated, in particular from two singular viewpoints. One is the effect of the axial bearing length. The bearing length does not affect dynamics related to the cylindrical mode. But the damping ratio, the natural frequency, and the critical speed of the conical mode are underestimated, if the effect of the bearing length is neglected, i.e., if the bearing force is assumed to be applied to the center of the bearing. The other is static instability in the very low-speed region. This instability occurs because the stiffness of the air bearing is not induced without rotation and is small at the very low-speed region, whereas the magnetic negative stiffness of the motor and/or magnetic bearing does occur even at zero speed. ◬

Acknowledgments. The author wishes to express his thanks to H. Makino and M. Takahashi for their useful suggestions.

References

1. J. M. Fleischer, M. R. Latta and M. E. Rabedeau, "Laser-optical system of the IBM 3800 printer," *IBM J. Res. Develop.* **21,** 479 (1977).
2. S. P. Sarraf, "Air spindle for laser scanner", *Proc. SPIE* **1079**, 443 (1989).
3. J. H. Vohr and C. Y. Chow, "Characteristics of herringbone-grooved, gas-lubricated journal bearings," *Trans. ASME D* **87,** 568 (1965).
4. V. Castelli and J. Pirvics, "Review of numerical methods in gas bearing film analysis," *Trans. ASME, J. Lubrication Tech.* 777 (1968).
5. B. J. Hamrock and D. P. Fleming, "Optimization of self-acting herringbone grooved journal bearings for maximum radial load capacity," in *Gas Bearing Symposium* (1971) Paper No. 13.
6. B. G. F. Boeker and B. Sternlicht, "Investigation of translatory fluid whirl in vertical machines," *Trans ASME* **13** (1956).
7. S. B. Malanoski, "Experiments on an ultrastable gas journal bearing," *Trans. ASME, F* **89,** 433 (1967).
8. R. E. Cunningham, D. P. Fleming and W. J. Anderson, "Experimental stability studies of the herringbone-grooved gas-lubricated journal bearing," *Trans ASME F* **91,** 52 (1969).
9. H. Kawamoto, "Stiffness analysis of magnetic bearing—radial stable stiffness of radial stable type magnetic bearing," *Bulletin JSME* **216,** 1654 (1983).
10. H. Kawamoto, "Magnetic bearing for high speed rotors," Ph.D. thesis, Tokyo Institute of Technology, 1983.
11. A. Tondl, *Some Problems of Rotor Dynamics,* Czechoslovak Academy of Sciences, Prague, 1965.
12. R. Gasch and H. Pfutzner, *Rotordynamik-eine Einfuhrung,* Springer-Verlag, Berlin, 1975.
13. V. V. Bolotin, *Nekonservativnyie Zadachi Teorii Uprugoi Ustoichivost,* Fizmatgiz, Moscow, 1962.
14. K. Ono, A. Iwama, M. Suzuki, T. Iwamura, Y. Itami and T. Hwang, "Analysis and design of radial and thrust bearing for polygonal scanner rotor-bearing system," *J. Trans. Jpn. Soc. Mech. Eng., C* **60,** 2670 (1996).
15. T. Hwang, K. Ono and Y. Itami, "Frequency response characteristics of unbalance and external excitations of scanner rotor supported by self-acting grooved-journal air bearings," *J. Trans. Jpn. Soc. Mech. Eng., C* **62,** 3915 (1996).